ChemComm

COMMUNICATION

View Article Online
View Journal | View Issue

Cite this: *Chem. Commun.*, 2021, 57, 6511

Received 17th May 2021,
Accepted 2nd June 2021

DOI: 10.1039/d1cc02588k

rsc.li/chemcomm

Closed bipolar electrode based fluorescence visualization biosensor for anti-interference detection of T-2 toxin†

Nan Hao,*[a] Yu Qiu,[a] Yaqi Li,[b] Jinwen Lu,[a] Xu Han,[c] Jing Qian [a] and Kun Wang *[ad]

A closed bipolar electrode (BPE) based fluorescence visualization biosensor was successfully constructed and used for anti-interference detection of T-2 toxin.

Fluorescence sensing has been widely applied due to high sensitivity and easy operation. New fluorescence materials and new sensing technologies are continuously developed.[1] But, in most present fluorescence biosensors, the fluorescence emitters and the sample solution are added together.[2] In practical detection, the complex solutes in the sample solution may affect the fluorescence signal. For example, some solutes may have good fluorescence activity and increase the background signal.[3]

All inorganic cesium lead halide perovskite semiconductors have become the new darlings of scientific research because of their excellent optical and electrical properties.[4] Although $CsPbX_3$ (X = Cl, Br, and I) QDs possess excellent fluorescence performance, there are few reports about their applications in fluorescence sensing because of the inherent instability in polar solvents.[5] A bipolar electrode (BPE) can generate electrochemical reactions at both extremities of the electrode with enough power in wireless mode, providing a powerful tool for exploring a variety of interesting applications.[6] In the closed BPE system, the sensing cell and the reporting cell are physical separated, only connected through a current path, which provides a promising approach to achieve aqueous solution analysis using $CsPbX_3$ QDs.[7]

Electrochromism is a phenomenon in which certain materials reversibly change their color or optical properties through a redox reaction under a small external voltage or current.[8] In previous work, we developed portable photo-electrochromic biosensors for the detection of contaminants in food and water based on the transition from Prussian blue (PB) to colorless Prussian white (PW).[9] In addition, switchable fluorescence can also be obtained using the spectral overlap between fluorescence emission and electrochromic materials.[10]

T-2 toxin has attracted considerable attention because of its high toxicity.[11] In this work, a closed BPE based fluorescence visualization biosensor was successfully constructed and used for anti-interference detection of T-2 toxin. Using the unique structure of the closed BPE system, the bio-recognition events between target molecules and aptamers in the sensing cell can affect the electrochromic process in the reporting cell through electron transfer, which further influences the fluorescence emission intensity because of the spectral overlap between the absorbance of PB and the fluorescence spectrum of $CsPbI_3$ (CPI) QDs. Possible interferences are avoided because there is no direct contact between the fluorescence emitters and complex solutes in the sample solution. This biosensor showed a good detection performance in the range of 1–100 ng mL^{-1} with a detection limit of 0.33 ng mL^{-1}. Moreover, it was successfully applied in beer sample detection.

The preparation of the carbon quantum dot (CQD)/g-C_3N_4/TiO_2 (CCNT) nanocomposite and CPI QDs and the fabrication process of the BPE are shown in the supporting information. As shown in Scheme 1A, the closed BPE was composed of two parts, the sensing cell modified with the CCNT composite and the reporting cell modified with PB/CPI QDs. Under light illumination, the photo-generated electrons generated by the sensing cell were transmitted to the reporting cell, thereby turning PB into Prussian white (PW). After adding the sample solution in the sensing cell, T-2 toxin molecules will bind to the aptamer and increase the steric hindrance, and then hinder the progress of the photoelectrochemical (PEC) reaction and lead to

[a] *School of Chemistry and Chemical Engineering, Jiangsu University, Zhenjiang 212013, P. R. China. E-mail: hn@ujs.edu.cn, wangkun@ujs.edu.cn*
[b] *School of Grain Science and Technology, Jiangsu University of Science and Technology, Zhenjiang, 212003, China*
[c] *Science and Technology on Space Physics Laboratory, Beijing, 10076, P. R. China*
[d] *Key Laboratory of Sensor Analysis of Tumor Marker, Ministry of Education, College of Chemistry and Molecular Engineering, Qingdao University of Science and Technology, Qingdao 266042, P. R. China*

† Electronic supplementary information (ESI) available. See DOI: 10.1039/d1cc02588k

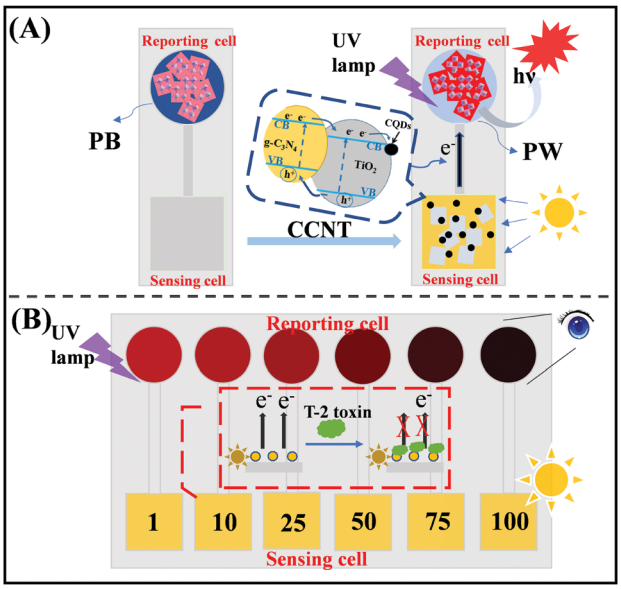

Scheme 1 Schematic illustration of the closed BPE based fluorescence visualization biosensor for anti-interference T-2 toxin detection.

a reduction in the number of electrons injected into the reporting cell, resulting in incomplete reduction of PB. The spectral overlap of the absorption spectrum and the fluorescence emission may cause internal filtering effects and resonance energy transfer. As shown in Fig. 1A, a wide absorption band (blue line) of PB covering the 500–800 nm range was collected, which overlapped the emission spectrum (red line) of the CPI QDs. After the PB film was reduced to PW, the absorbance was greatly reduced (black line). As shown in Fig. 1D, the emission of the CPI QDs was quenched due to the spectral overlap between PB and CPI QDs. Significant fluorescence emission was obtained after turning PB into PW (Fig. 1E). Finally, based on the relationship between the fluorescence intensity of the reporting cell and targets of different concentrations added into the sensing cell (Scheme 1B), a visual biosensor was constructed for the detection of T-2 toxin. Possible interferences are successfully avoided because there is no direct contact between the fluorescence emitters and complex solutes in the sample solution.

Uniform cubic $CsPbI_3$ QDs of approximately 10 nm can be observed in the transmission electron microscope (TEM) images (Fig. 2B). The inset shows a photo of $CsPbI_3$ QDs with strong fluorescence under UV light.[12] As shown in Fig. 2A, the

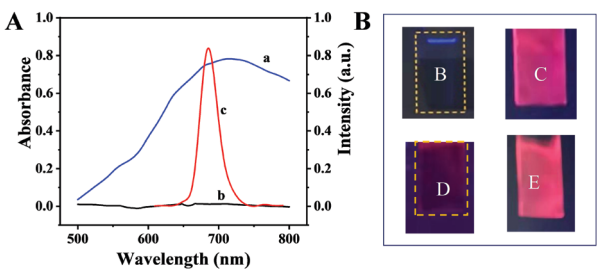

Fig. 1 (A) Absorption spectra of the PB layer (blue line) and PW layer (black line); and fluorescence spectrum of CPI QDs (red line). Photos of (B) PB, (C) CPI, (D) PB + CPI and (E) PW + CPI under UV light.

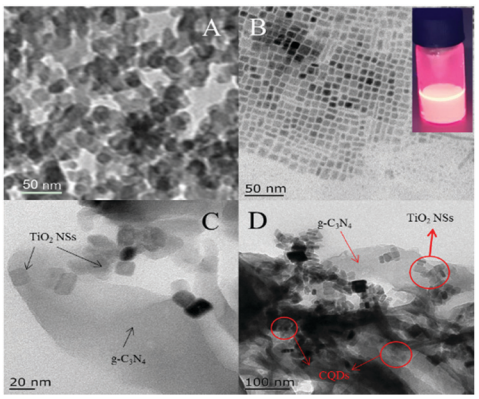

Fig. 2 TEM image of (A) CQDs, (B) $CsPbI_3$ QDs, (C) CNT and (D) CCNT.

size of the CQDs is mostly 4–8 nm.[13] Fig. 2C shows a TEM image of CNT. TiO_2 NSs with a length and a width of about 20 nm are deposited on two-dimensional irregular g-C_3N_4 flakes. According to previous reports,[14] this face-to-face contact can increase the contact area and facilitate photo-generated electron transfer. The TEM image of CCNT is shown in Fig. 3D. TiO_2 NSs are deposited on large g-C_3N_4 sheets, and a small amount of CQDs are scattered on the g-C_3N_4 sheets and TiO_2 NSs. The scanning electron microscope (SEM) image, X-ray diffraction (XRD) and X-ray photoelectron spectroscopy (XPS) are shown in the supporting information. The SEM image and energy dispersive spectroscopy (EDS) (Fig. S1, ESI†) further confirm the presence of g-C_3N_4 and TiO_2 in CCNT. The XRD patterns of pure g-C_3N_4, pure TiO_2 NSs and CCNT are shown in Fig. S2A (ESI†) and the UV-visible spectrum and PL spectrum of $CsPbI_3$ QDs are shown in Fig. S2B (ESI†). In order to further explore the chemical structure of CCNT, XPS analysis was performed (Fig. S3, ESI†). The results confirm the simultaneous presence of CQDs, g-C_3N_4 and TiO_2 NSs in the CCNT samples. The ultraviolet-visible diffuse reflection spectrum (DRS) and

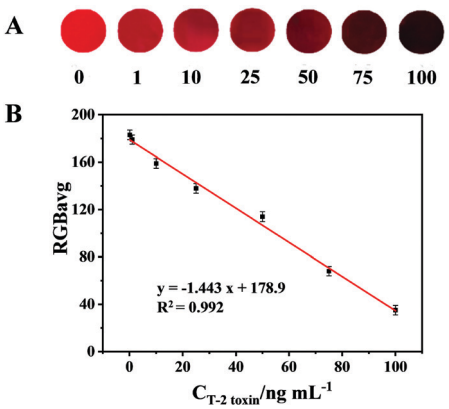

Fig. 3 Closed bipolar visualization strategy for detecting different concentrations of T-2 toxin from 1 to 100 ng mL^{-1}. (A) Photographs of reporting cells in different concentrations of T-2 toxin: 0 ng mL^{-1}, 1 ng mL^{-1}, 10 ng mL^{-1}, 25 ng mL^{-1}, 50 ng mL^{-1}, 75 ng mL^{-1}, and 100 ng mL^{-1}. (B) Linear relationship between the T-2 toxin concentration and the RGB value of the reporting cells.

estimated band gap of TiO_2 NSs, g-C_3N_4 and CCNT are shown in the supporting information (Fig. S4, ESI†), which indicate that the CCNT composites have improved the utilization of visible light.

The photocurrent responses and electrochemical impedance spectroscopy (EIS) spectra of these materials are shown in Fig. S5 (ESI†), which demonstrates that the CCNT composites have excellent photoelectric properties under visible light. The photoelectrons generated in the sensing cell were transferred to the reporting cell through the BPE conductive layer, which changed the color of PB and thus changed the fluorescence intensity of CPI. As shown in Fig. 3A, as the T-2 toxin concentration increased from 1 ng mL^{-1} to 100 ng mL^{-1}, the fluorescence intensity of CPI gradually weakened, indicating that the electrons generated in the sensing cell were increasingly insufficient to turn PB into PW. As a result, the fluorescence quenching effect of PB on CPI was more and more obvious. In order to further confirm the effect of steric hindrance on electron transfer, the Nyquist diagrams of different processes were recorded and are shown in Fig. S5C (ESI†). When the T-2 toxin was introduced, R_{et} increased from approximately 230 Ω to 380 Ω. To quantify the T-2 toxin concentration, the RGB value of the reporting cells was analyzed using PS software, which increased with increasing T-2 toxin concentration. A linear relationship in the range of 1 to 100 ng mL^{-1} with a detection limit of 0.33 ng mL^{-1} was obtained (Fig. 3B). The above results showed that the visual biosensor designed to detect T-2 toxin had good detection performance. We compared our work with other reported methods and the results are exhibited in Table S2 (ESI†). Fig. S6 (ESI†) demonstrates that the biosensor has good selectivity and stability. The performance of this developed visual biosensor in actual sample analysis was investigated with a beer sample by standard addition methods (Table S1, ESI†).

In conclusion, a closed BPE based fluorescence visualization biosensor system using highly efficient $CsPbI_3$ QDs was successfully constructed. Based on the good fluorescence performance of $CsPbI_3$ QDs, Prussian blue to Prussian white transition characteristics and electrochromic principle, this developed biosensor was applied to the detection of T-2 toxin in beer samples. Compared with traditional fluorescence biosensors, this work developed a new approach to reduce possible interferences from complex solutes in the sample solution, which can provide new inspiration for the further development of fluorescence sensing.

Nan Hao: experimental guidance and writing. Yu Qiu: investigation, validation, formal analysis. Yaqi Li: experimental support. Jinwen Lu: experimental support. Xu Han: formal analysis. Jing Qian: data curation. Kun Wang: funding acquisition and writing – review & editing.

This work was supported by the National Natural Science Foundation of China (No. 21876068, 31901799 and 21675066), and Project of Faculty of Agricultural Equipment of Jiangsu University (NZXB20200210).

Conflicts of interest

There are no conflicts to declare.

References

1 (*a*) S. Govindaraju, A. S. Reddy, J. Kim and K. Yun, *Appl. Surf. Sci.*, 2019, **498**, 10; (*b*) S. Shanmugaraju, D. Umadevi, L. M. Gonzalez-Barcia, J. M. Delente, K. Byrne, W. Schmitt, G. W. Watson and T. Gunnlaugsson, *Chem. Commun.*, 2019, **55**, 12140–12143; (*c*) S. Y. Wu, H. Min, W. Shi and P. Cheng, *Adv. Mater.*, 2020, **32**, 14.

2 (*a*) S. S. Tan, S. J. Kim and E. T. Kool, *J. Am. Chem. Soc.*, 2011, **133**, 2664–2671; (*b*) Y. Jeong, Y.-M. Kook, K. Lee and W.-G. Koh, *Biosens. Bioelectron.*, 2018, **111**, 102–116; (*c*) L. Long, Y. Han, X. Yuan, S. Cao, W. Liu, Q. Chen, K. Wang and Z. Han, *Food Chem.*, 2020, **331**, 127359.

3 (*a*) Y. Shi, Y. Sun, X. Qu, L. Zhou, T. Yue and Y. Yuan, *Food Chem.*, 2021, **347**, 129069; (*b*) N. H. T. Tran, T. B. Phan, T. T. Nguyen and H. Ju, *Biosens. Bioelectron.*, 2021, **176**, 112900.

4 (*a*) M. Abdi-Jalebi, Z. Andaji-Garmaroudi, S. Cacovich, C. Stavrakas, B. Philippe, J. M. Richter, M. Alsari, E. P. Booker, E. M. Hutter, A. J. Pearson, S. Lilliu, T. J. Savenije, H. Rensmo, G. Divitini, C. Ducati, R. H. Friend and S. D. Stranks, *Nature*, 2018, **555**, 497–501; (*b*) K. Lin, J. Xing, L. N. Quan, F. P. G. de Arquer, X. Gong, J. Lu, L. Xie, W. Zhao, D. Zhang, C. Yan, W. Li, X. Liu, Y. Lu, J. Kirman, E. H. Sargent, Q. Xiong and Z. Wei, *Nature*, 2018, **562**, 245–248; (*c*) H. Tsai, R. Asadpour, J.-C. Blancon, C. C. Stoumpos, O. Durand, J. W. Strzalka, B. Chen, R. Verduzco, P. M. Ajayan, S. Tretiak, J. Even, M. A. Alam, M. G. Kanatzidis, W. Nie and A. D. Mohite, *Science*, 2018, **360**, 67; (*d*) Y. Cao, Z. Zhang, L. Li, J.-R. Zhang and J.-J. Zhu, *Anal. Chem.*, 2019, **91**, 8607–8614.

5 (*a*) C. Chen, Q. Cai, F. Luo, N. Dong, L. Guo, B. Qiu and Z. Lin, *Anal. Chem.*, 2019, **91**, 15915–15921; (*b*) Y. Zhu, F. Li, Y. Huang, F. Lin and X. Chen, *Anal. Chem.*, 2019, **91**, 14183–14187.

6 (*a*) S. E. Fosdick, K. N. Knust, K. Scida and R. M. Crooks, *Angew. Chem., Int. Ed.*, 2013, **52**, 10438–10456; (*b*) M. Hasheminejad, Y. Fang, M. Li, Y. Jiang, W. Wang and H.-Y. Chen, *Angew. Chem., Int. Ed.*, 2017, **56**, 1629–1633; (*c*) L. Zhang, B. Gupta, B. Goudeau, N. Mano and A. Kuhn, *J. Am. Chem. Soc.*, 2018, **140**, 15501–15506; (*d*) H. B. Aiyappa, P. Wilde, T. Quast, J. Masa, C. Andronescu, Y.-T. Chen, M. Muhler, R. A. Fischer and W. Schuhmann, *Angew. Chem., Int. Ed.*, 2019, **58**, 8927–8931; (*e*) N. Shida and S. Inagi, *Chem. Commun.*, 2020, **56**, 14327–14336.

7 N. Hao, J. Lu, Z. Dai, J. Qian, J. Zhang, Y. Guo and K. Wang, *Electrochem. Commun.*, 2019, **108**, 106559.

8 (*a*) R. J. Mortimer, *Chem. Soc. Rev.*, 1997, **26**, 147–156; (*b*) Y. Wang, E. L. Runnerstrom and D. J. Milliron, in *Annual Review of Chemical and Biomolecular Engineering*, ed. J. M. Prausnitz, Annual Reviews, Palo Alto, 2016, vol. 7, pp. 283–304.

9 (*a*) Z. Dai, N. Hao, M. Xiong, X. Han, Y. Zuo and K. Wang, *Anal. Chem.*, 2020, **92**, 13604–13609; (*b*) N. Hao, Z. Dai, X. Meng, R. Hua, J. Lu and K. Wang, *Sens. Actuators, B*, 2020, **306**, 127594.

10 (*a*) L. Jin, Y. Fang, L. Shang, Y. Liu, J. Li, L. Wang, P. Hu and S. Dong, *Chem. Commun.*, 2013, **49**, 243–245; (*b*) Y. Zhai, H. Zhang, L. Zhang and S. Dong, *Nanoscale*, 2016, **8**, 9493–9497; (*c*) H. Xing, X. Zhang, Q. Zhai, J. Li and E. Wang, *Anal. Chem.*, 2017, **89**, 3867–3872; (*d*) J. Z. Sun, Y. Li, J. K. Sun, Z. J. Zhu, Y. L. Zhai and S. J. Dong, *Chem. Commun.*, 2019, **55**, 12060–12063.

11 Y. Li, Z. Wang, R. C. Beier, J. Shen, D. De Smet, S. De Saeger and S. Zhang, *J. Agric. Food Chem.*, 2011, **59**, 3441–3453.

12 G. Nedelcu, L. Protesescu, S. Yakunin, M. I. Bodnarchuk, M. J. Grotevent and M. V. Kovalenko, *Nano Lett.*, 2015, **15**, 5635–5640.

13 J. Liu, Y. Liu, N. Liu, Y. Han, X. Zhang, H. Huang, Y. Lifshitz, S.-T. Lee, J. Zhong and Z. Kang, *Science*, 2015, **347**, 970.

14 Y. Li, X. H. Feng, Z. X. Lu, H. Yin, F. Liu and Q. J. Xiang, *J. Colloid Interface Sci.*, 2018, **513**, 866–876.